Weyl solitons in three-dimensional optical lattices

Ce Shang, Yuanlin Zheng, and Boris A. Malomed

Phys. Rev. A **97**, 043602 — Published 3 April 2018

DOI: 10.1103/PhysRevA.97.043602

Weyl solitons in three-dimensional optical lattices

Ce Shang,[1, 2, *] Yuanlin Zheng,[1, 2] and Boris A. Malomed[3]

[1] *The State Key Laboratory of Advanced Optical Communication Systems and Networks, Shanghai Jiao Tong University, Shanghai 200240, China*

[2] *Key Laboratory for Laser Plasma (Ministry of Education), Collaborative Innovation Center of IFSA, School of Physics and Astronomy, Shanghai Jiao Tong University, Shanghai 200240, China*

[3] *Department of Physical Electronics, School of Electrical Engineering, Faculty of Engineering, Tel Aviv University, Tel Aviv 69978, Israel*

Weyl fermions are massless chiral quasiparticles existing in materials known as Weyl semimetals. Topological surface states, associated with the unusual electronic structure in the Weyl semimetals, have been recently demonstrated in linear systems. Ultracold atomic gases, featuring laser-assisted tunneling in three-dimensional optical lattices, can be used for the emulation of Weyl semimetals, including nonlinear effects induced by the collisional nonlinearity of atomic Bose-Einstein condensates. We demonstrate that this setting gives rise to topological states in the form of Weyl solitons at the surface of the underlying optical lattice. These nonlinear modes, being exceptionally robust, bifurcate from linear states for a given quasi-momentum. The Weyl solitons may be used to design an efficient control scheme for topologically-protected unidirectional propagation of excitations in light-matter-interaction physics. After the recently introduced Majorana and Dirac solitons, the Weyl solitons proposed in this work constitute the third (and the last) member in this family of topological solitons.

I. INTRODUCTION

Three species of fermions, of the Dirac [1], Majorana [2, 3] and Weyl types [4–6], are cornerstones of the relativistic quantum-field theory. On the other hand, Weyl semimetals, which enable the realization of the Weyl fermions, is opening up a new chapter of condensed-matter physics. Weyl points, the signature of the respective topological charge, are produced by the Hamiltonian $H = v_x k_x \sigma_x + v_y k_y \sigma_y + v_z k_z \sigma_z$, where v_j, k_j and σ_j, with $j = x, y, z$, are group velocities, momentum components, and Pauli matrices, respectively. With linear dispersion in all the three dimensions in its vicinity [7–11], these nodal points in the momentum space are realized as magnetic monopoles in the **k**-space. The topological invariant of the Weyl semimetal may be determined by the sign chirality, defined as $\chi = \text{sign}\,(v_x v_y v_z)$, or the integral of the Berry curvature on a closed manifold enclosing the Weyl point. The gapless topological states built of bulk low-energy electrons also feature the existence of the Weyl semimetal. Aside from solid-state electronic materials, the rapid development of the technique based on synthetic magnetic fields in ultracold atomic gases [12, 13] and possibilities to precisely control properties of Bose-Einstein condensates (BECs) [14] offer an efficient platform for investigating topological phenomena and novel states of matter. In particular, lattice models make it possible to handle pseudospin components of the wave functions by modifying the lattice geometry, which also may result in the emergence of Weyl points [15–17]. The unusual structure of the wave functions near these points gives rise to a plenty of notable topological properties and stimulates ongoing research in various fields of physics.

The topological phenomena and relativistic particles mentioned above are generally produced by linear systems. Nonlinearity also essentially affects a variety of phenomena in physics, such as coherent control of excitations [18], bistability [19], soliton formation [20–23], harmonic generation and frequency conversion [24], and many others. Effects of nonlinearity on edge states, including prediction of solitons, were recently studied in topological insulators [25–27]. However, the impact of nonlinearities on Weyl semimetals, associated with either nonlinear effects in surface-state propagation or interparticle interactions was not explored yet. In the present work, we address this issue, considering competing repulsive and attractive interactions [28–33] between atoms in synthetic magnetic fields [34, 35], which is similar to the interplay of self-defocusing and focusing nonlinearities in optics. The objective of our analysis is to build soliton-like surface states, in the full three-dimensional (3D) form, in optical Weyl lattices emulating the Weyl metals. These nonlinear lattices can be utilized to study interplay between the nonlinearity and topologically protected surface states. We find that soliton modes bifurcate from linear periodic surface states. We also find that these Weyl solitons may travel along the surface without notable deformations, featuring extremely low radiation loss. The Weyl solitons, after the very recently reported Dirac solitons [36] and Majorana solitons[37], are the third and also the last member in the family of topological solitons, finally hosting a reunion in nonlinear physics.

* shangce1989@sjtu.edu.cn

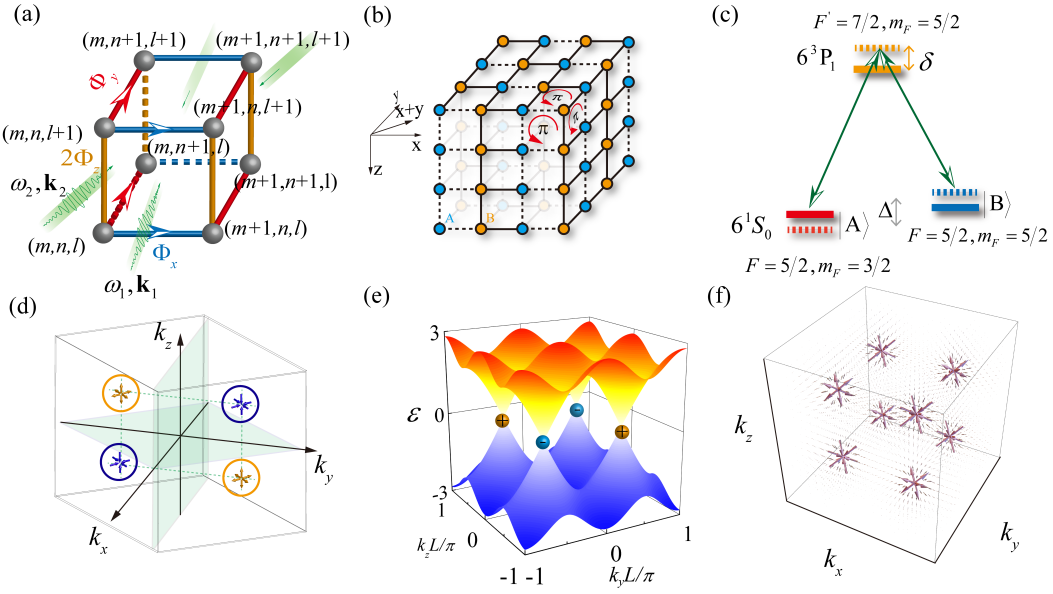

FIG. 1. (a) Optical-lattice potentials formed by superimposing two standing waves, and the configuration of gauge fields defined on bonds of the cubic lattice with the corresponding coordinates. (b) A sketch of the 3D cubic lattice with phase-driven hopping along x and z directions, which possesses Weyl points in the momentum space. Amplitudes of tunneling along the lattice sites alternately carry a complex phase shown as dashed (solid) lines, illustrating hopping with an acquired phase π (0). The unit cell can be constructed, using two pseudospin sites marked by orange and blue colors. (c) The Raman coupling scheme for engineering the required tunneling along each axis. The detuning Δ matches the frequency offset of the corresponding Raman beams. (d) The positions of the Weyl points in the Brillouin zone of the 3D Hamiltonian in the reciprocal lattice and their chiralities are indicated by blue and orange arrow sets. (e) The band structure with signs of the Weyl points in the (k_y, k_z) plane, at $k_x = 0$. (f) Distribution of the Berry curvature of Weyl nodes in momentum space with the opposite chiralities.

II. THE LINEAR MODEL

Gauge fields play an essential part in various areas of modern physics [38]. In particular, the Harper Hamiltonian in the tight-binding limit, based on gauge fields, describes the dynamics of particles in a magnetic field with a background lattice. This Hamiltonian has been already shown to exhibit a fascinating fractal band structure which is called the "Hofstadter butterfly" [39]. The particular Harper Hamiltonian was recently proposed for the realization of the Weyl states [40] in ultracold atoms.

An optical Weyl lattice may be induced by the electric dipole interaction between atoms and the electric field of an optical standing wave. As shown in Fig. 1(a), two running-wave Raman laser beams with frequencies and wave vectors $[\omega_\alpha, \mathbf{k}_\alpha]$, $\alpha = 1, 2$, induce a spatially dependent complex tunneling by the position-dependent modulation, and generate strong synthetic magnetic fields. Due to this modulation, the tunneling matrix element consequently picks up a Peierls phase, which originates from the propagator of an electron in the magnetic field. With the precise control of the laser field, one can efficiently engineer the Peierls phase and redefine atom hopping by adding an Aharonov-Bohm-like phase, Φ, which is equal to the sum of the Peierls phases, accumulated in the course of tunneling around the plaquette [41]. The plaquette, regarded as a gauge invariant, is defined modulo the dimensionless magnetic flux quantum of 2π piercing a lattice. In Fig. 1(b), we introduce a uniform fully tunable effective flux and the lattice built of two sublattices (A and B, which build a unit cell), which give rise to pseudospins with opposite magnetic moments. Our coupling scheme directly creates a non-Abelian $SU(2)$ gauge field that results in opposite magnetic fields for quasiparticles. Thus, a 3D cubic lattice can be constructed with laser-assisted tunneling along x and z directions. For resonant tunneling [42, 43], the time averaging over the rapidly oscillating terms yields an effective 3D Hamiltonian:

$$H = -\sum_{\mathbf{r},\sigma,\tau} (J_x e^{-i\Phi_{\mathbf{r}+\hat{x},\mathbf{r}}} a^\dagger_{\mathbf{r}+\hat{x},\sigma} a_{\mathbf{r},\tau} + J_y a^\dagger_{\mathbf{r}+\hat{y},\sigma} a_{\mathbf{r},\tau} + J_z e^{-i\Phi_{\mathbf{r}+\hat{z},\mathbf{r}}} a^\dagger_{\mathbf{r}+\hat{z},\sigma} a_{\mathbf{r},\tau} + \text{H.c.}). \quad (1)$$

Here, $J_{x,y,z}$ are tunneling amplitudes, $\sigma, \tau = A, B$ label the two pseudospin components, $a^\dagger_{\mathbf{r},\sigma,\tau}$ and $a_{\mathbf{r},\sigma,\tau}$ are the creation and annihilation operators on site $\mathbf{r} = (m, n, l)$, and $\Phi_{\mathbf{r}} = \delta\mathbf{k} \cdot R_{m,n,l} = m\Phi_x + n\Phi_y + l\Phi_z$ denote the nontrivial hopping phases, associated with positions $R_{m,n.l}$=$mL\hat{x} + nL\hat{y} + lL\hat{z}$ and momentum difference $\delta\mathbf{k}$=$\mathbf{k}_1 - \mathbf{k}_2$, where m, n, l are integers, and $\hat{x}, \hat{y}, \hat{z}$ are unit vectors along the x, y, z direction, respectively. The lattice spacing is L. We select the appropriate directions

such that $(\Phi_x, \Phi_y, \Phi_z) = \pi(1, 1, 2)$.

The experiment can be performed in quantum degenerate Fermi gases of ^{173}Yb in the presence of a uniform magnetic field $\mathcal{B}$ [44, 45]. We consider the $6^1S_0 \rightarrow 6^3P_1$ transition with one excited state $\left|F' = 7/2, m_F = 5/2\right\rangle$ and two ground states $|F = 5/2, m_F = 3/2\rangle$, $|F = 5/2, m_F = 5/2\rangle$. , We set the frequency difference $\omega_1 - \omega_2 \approx \Delta$ ($\Delta = g_F \mu_{\mathcal{B}} \mathcal{B}$), so that the dressed ground states are nearly degenerate, g_F is the hyperfine Landé factor, $\mu_{\mathcal{B}}$ is the Bohr magneton, and m_F is the projection of the atomic angular momentum along the magnetic field. The two-photon detuning is δ. In the presence of large detuning $\Delta \gg \Omega, \delta$, we can adiabatically eliminate the excited state and consider the atomic motions in the ground-state manifold, to derive the hopping term $J = \Omega^2/\delta$, where Ω is the strength of the Raman coupling between the ground and excited states.

It is relevant to mention here that the proposed scheme may be actually realized more straightforwardly for bosonic systems, such as chiral vortices in an interacting bosonic quantum fluid [46]. Relevant details of the bosonic setting will be considered in detail elsewhere.

In the quasi-momentum representation, the present setting amounts to the 3D Harper Hamiltonian for two sublattices: $H(\mathbf{k}) = -2\left[J_y \cos(k_y L)\sigma_x + J_x \sin(k_x L)\sigma_y - J_z \cos(k_z L)\sigma_z\right]$. In the first Brillouin zone (BZ) in Fig. 1(d) the two energy bands $\varepsilon(k) = \pm 2\sqrt{J_x^2 \sin^2(k_x L) + J_y^2 \cos^2(k_y L) + J_z^2 \cos^2(k_z L)}$ touch at $(k_x, k_y, k_z) = (0, \pm\pi/2L, \pm\pi/2L)$. Figure 1(e) depicts the energy spectra in the BZ, Weyl points and their chiralities. Hamiltonian $H(\mathbf{k})$ may be compactly written as $H = \mathbf{d} \cdot \boldsymbol{\sigma}$, where vector $\mathbf{d}$ has components $d_x = -2J_y \cos(k_y L)$, $d_y = -2J_x \sin(k_x L)$, and $d_z = 2J_z \cos(k_z L)$. The Weyl point is a source of the monopole magnetic field. Here, paired Weyl points with opposite chiralities may be viewed as a monopole-antimonopole pair in the momentum space. To show these points, we derive the Berry curvature for the lowest band [47]:

$$F^a = \epsilon_{abc} F_{bc} = \epsilon_{abc}\left[\frac{1}{2d^3}\mathbf{d} \cdot \left(\frac{\partial \mathbf{d}}{\partial k_b} \times \frac{\partial \mathbf{d}}{\partial k_c}\right)\right], \quad (2)$$

where the three components of $\mathbf{F}(\mathbf{k})$ are

$$\begin{aligned} F^x &= -8J_x J_y J_z \sin(k_x L)\sin(k_y L)\sin(k_z L)/D(\mathbf{k}) \\ F^y &= 8J_x J_y J_z \cos(k_x L)\cos(k_y L)\sin(k_z L)/D(\mathbf{k}) \\ F^z &= 8J_x J_y J_z \cos(k_x L)\sin(k_y L)\cos(k_z L)/D(\mathbf{k}) \end{aligned}, \quad (3)$$

where $D(\mathbf{k}) = \left[4J_x^2 \sin^2(k_x L) + 4J_y^2 \cos^2(k_y L) + 4J_z^2 \cos^2(k_z L)\right]^{3/2}$. In Fig. 1(f), arrows show that the flux of the Berry curvature $\mathbf{F}(\mathbf{k})$ flows from one monopole to the other, thus defining nontrivial topological properties of a topological semimetal, where the Weyl points behave as a sink and source.

The dispersions around the Weyl points are locally linear and described by $H(\mathbf{q}) = \sum_{i,j=[x,y,z]} v_{ij} q_i \sigma_j$, where $\mathbf{q}$ is the displacement momentum with respect to the momentum of the node, v_{ij} are elements of a 3×3 matrix

$$\begin{pmatrix} 0 & -2J_x L & 0 \\ \pm 2J_y L & 0 & 0 \\ 0 & 0 & \pm 2J_z L \end{pmatrix}, \quad (4)$$

and the chirality, which determines the Weyl points, may be defined as $\chi = \mathrm{sign}(\det[v_{i,j}])$.

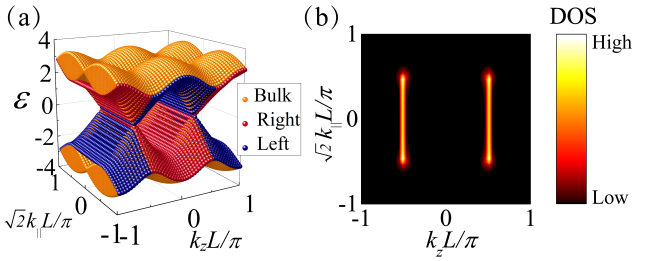

FIG. 2. (a) The energy spectrum of the slab, $\varepsilon(k_\parallel, k_z)$, with open boundary conditions. The Weyl points are connected with Fermi arcs in the momentum space. Two sheets of surface states, corresponding to the two surface states localized at the right and left sides of the slab, are Fermi arcs shown by red and blue, respectively. (b) Zero-energy momentum spectrum of surface states showing the trajectory of the surface Fermi arc, representing arcs connecting Weyl points with opposite chiralities and the intersections of the two dispersion sheets.

Weyl semimetals imply the existence of topological surface states in the form of Fermi arcs in the momentum space. The appearance of Fermi arcs is expected whenever the projections of the Weyl points onto the surface of the cut (open boundary condition) do not coincide. Furthermore, the states are highly localized on the surface, and their group velocity will show a specific propagation direction for each surface. To observe the surface state induced by the topological properties of the Fermi arcs, we consider a material maintaining translational invariance in all the three directions. The bulk-boundary correspondence suggests that there exist topological surface modes propagating along the interface of the lattice. We take a slab cut orthogonally to the $\hat{x} - \hat{y}$ direction (infinite along the $\hat{z}$ and $\hat{x} + \hat{y}$ directions) in. The slab is considered as a 2D Bravais lattice possessing each good quantum number along $k_\parallel$ or k_z .The unit vectors of the Bravais lattice of the slab are $\mathbf{a}_1 = L(\hat{x} + \hat{y})$ and $\mathbf{a}_2 = L\hat{z}$. A generic $\mathbf{k}$-point in the BZ is expressed as $\mathbf{k} = k_\parallel(\hat{x} + \hat{y})/\sqrt{2} + k_z \hat{z}$. Thus, the projection of Weyl points onto the slab surface are at $(k_\parallel, k_z) = (\pm\pi/\sqrt{2}L, \pm\pi/L)$, and $\varepsilon(k_\parallel, k_z)$ is plotted in Fig. 2(a). The red and blue modes are surfaces states localized, respectively, at the right (RT) and left (LT) edges of the lattice. Specifically, the zero-energy momentum spectrum (ε=0) is calculated using Eq. 5, which is constructed in terms of the exact eigenstates of

Hamiltonian [48, 49]:

$$\rho\left(\varepsilon,\mathbf{k}\right)=-\frac{1}{\pi}\mathrm{Im}Tr\left[\frac{1}{\varepsilon-H\left(\mathbf{k}\right)+i0^{+}}\right]. \tag{5}$$

Figure 2(b) shows two open-line segments connecting four projected Weyl nodes with four opposite chiralities, implying the existence of two separate surface Fermi arcs. To detect the Weyl points, the linear spectra along the three directions can be measured by means of the momentum-resolved radio-frequency spectroscopy, which has been utilized for the observation of the Dirac cone in atomic gases [50, 51].

III. THE NONLINEAR MODEL

Now, we focus on the transport characteristics of the surface mode in the present system. The time evolution can be described by a scaled system of coupled Eq. for the A and B components of the spinor wave function $\mathbf{\Psi}=\left(\psi^{A}_{m,n,l},\psi^{B}_{m,n,l}\right)^{T}$:

$$i\frac{d\psi^{\sigma}_{m,n,l}}{dt}=\sum_{\tau}H^{\sigma,\tau}\psi^{\tau}_{m,n,l}. \tag{6}$$

To introduce the bulk-edge correspondence , we first address the spectrum of linear modes that are periodic along the z-axis and cut in the $\hat{x}+\hat{y}$ and $\hat{x}-\hat{y}$ direction near the edge. These modes are Bloch functions $\psi^{\sigma}_{m,n,l}=u^{\sigma}_{m,n,l}e^{i\varepsilon t+ik_{z}lL}$, where k_z is the Bloch momentum, ε is the energy eigenvalue, and the corresponding momentum width of the BZ is given by $2\pi/L$. Based on the similarity to multilayer structures which realize the 3D Weyl-semimetal phase [52], we treat the Weyl lattice as a set of identical plane layers. The periodicity along the z direction insures that k_z as an appropriate quantum number. For each fixed k_z, the 3D system can be reduced to an effective 2D one with a unit cell in the (x,y) plane [53]. The respective 2D Hamiltonian, $H^{2D}_{k_z}$, is parameterized by k_z. The nonzero Chern number ±2 of $H^{2D}_{k_z}$ implies the existence of edge states at the boundary of finite systems. On the 2D BZ parallel to k_z, the chiral surface states wrap around the full 2D BZ forming Fermi arcs [54–56]. Utilizing the 2D equivalence, stationary states of Eqs. (6) under open boundary condition corresponding to H_{k_z} are denoted as

$$\sum_{\tau}\left(e^{-ik_{z}L}H^{\sigma,\tau}_{m,n,l\ -1}+H^{\sigma,\tau}_{m,n,l}+e^{ik_{z}L}H^{\sigma,\tau}_{m,n,l\ +1}\right)u^{\tau}_{m,n,l}=\varepsilon u^{\sigma}_{m,n,l}. \tag{7}$$

Here, indices m,n enumerate the unit cells in the x and y directions, and l denotes a specific layer along the z-axis. For a single atom, energy eigenstates are Bloch wave functions, or an appropriate superposition of Bloch states which are well localized on individual lattice sites. To simplify the notation and relate the indices to the coordinates, $\psi^{\sigma}_{m,n,l}=u^{\sigma}_{m,n,l}e^{i\varepsilon t+ik_{z}lL}$ can be rewritten as $\psi_{\sigma}\left(x,y,z\right)=e^{i\varepsilon t+ik_{z}z}u_{\sigma}\left(x,y,z\right)$. A representative spectrum for the lattice with the surface states is shown in Fig. 3(a) in the form of the energy-momentum diagrams for the $[-\pi/L,\pi/L]$ interval by solving Eqs. (7). Due to the spinor character of the model, the spectrum consists of two groups of bands. The spectrum shows two Weyl points at $\pm k_zL/2\pi$, where the upper and lower bands touch each other. In Fig. 3(b), we plot the dispersion

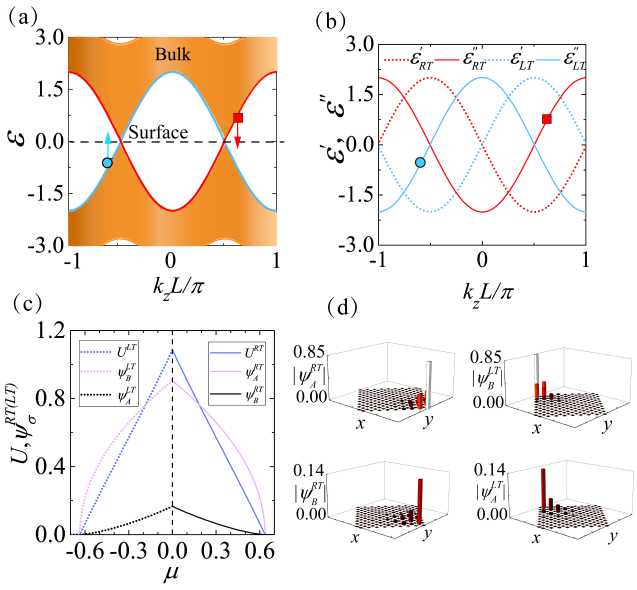

FIG. 3. (a) Orange parts correspond to the modes residing in the bulk of the lattice, while red and blue lines indicate surface states belonging to different branches. (b) First- and second-order derivatives of the energy of linear surface states versus momentum k_z. Red square and blue circle denote parameters corresponding to the modes at $k_z=-0.4\pi,0.6\pi$. (c) Norm U_σ per z-period and peak amplitudes ψ_σ of pseudospin components σ versus μ for the nonlinear surface states. The power and amplitude of the nonlinear modes bifurcate from the zero-intensity point for $k_z=-0.4\pi,0.6\pi$. Solid and dotted curves denote the amplitude of $\psi^{RT(LT)}_{\sigma}$ component. (d) The transverse profile of A and B components per z-period of the nonlinear surface state at right and left corner of the lattice.

coefficient ε'' as a function of k_z corresponding to different linear surface states. RT (LT) branches in the momentum intervals presenting the localized states near the right (left) edge are denoted by the red (blue) color. All such intervals for every linear surface mode give rise to surface solitons which are investigated below. For every branch, there exist two unique k_z values where dispersion ε'' vanishes and wave packets with a broad envelope may evolve almost without broadening even in the linear limit, due to the vanishing of the dispersion near the Weyl points.

To study dynamics of the nonlinear surface excitations and capture transport characteristics in the nonlinear model, nonlinear terms are added to Eqs. (6). Hence, the nonlinear evolution of the vector wave function with

nonlinear interaction is governed by the following Eqs.:

$$i\frac{d\psi^{\sigma}_{m,n,l}}{dt}=\sum_{\tau}H^{\sigma,\tau}\psi^{\tau}_{m,n,l}+N^{\sigma}\left(\psi^{\sigma}_{m,n,l}\right)\psi^{\sigma}_{m,n,l}, \quad (8)$$

where H_σ maintains the form of the coupling matrix of the lattice, and $N^{\sigma}\left(\psi^{\sigma}_{m,n,l}\right)$ represents the diagonal matrix with nonlinear elements [36, 57, 58]:

$$\left[N^{\sigma}\left(\psi^{\sigma}_{m,n,l}\right)\right]=g^{\sigma}\left(\left|\psi^{\sigma}_{m,n,l}\right|^{2}\right). \quad (9)$$

Here, self-interaction nonlinearity can be achieved by applying the mean-field theory (variables ψ_σ represent large clusters trapped at different sites of the lattice, rather than individual atoms). Although the Pauli principle does not allow the direct self-interaction, an effective self-interaction may be induced via the local-field effect, i.e., local deformation of the optical lattice by the atomic gas [59–61]. By applying the continuum approximation [62, 63]($k_z d \ll 1$, d is the step size of the Taylor expansion), the diffraction coefficients along the z-axis of the two components are denoted as $\gamma_z^{\sigma}=\pm d^2\cos\left(k_z L\right)$. Under this approximation, the type of diffraction can be compensated by the nonlinearity. For given k_z, the nonlinear coefficient g^σ in Eqs. (9) is rescaled to be $g^{\sigma}=\pm 1$ for repulsive and attractive interatomic interactions, respectively [64]. Nonlinear solutions are introduced in the same form as the linear ones,

$$\psi^{\sigma}_{m,n,l}=\phi^{\sigma}_{m,n,l}e^{i\mu t+ik_z lL}, \quad (10)$$

which may also be written as: $\psi_\sigma\left(x,y,z\right)=u_\sigma\left(x,y,z\right)e^{i\mu t+ik_z z}$. The substitution of ansatz (10) in Eqs. (8) leads to the stationary version of the nonlinear Eqs.:

$$\mu\phi^{\sigma}_{m,n,l}=\sum_{\tau}H^{\sigma,\tau}\phi^{\tau}_{m,n,l}+N^{\sigma}\left(\phi^{\sigma}_{m,n,l}\right)\phi^{\sigma}_{m,n,l}, \quad (11)$$

Because the nonlinearity in our model dominates over the interaction between the pseudospin components, nonlinear solutions exist when nonlinearity-induced energy eigenvalue, μ, does not fall into the bulk band (i.e., it belongs to the spectral gap), and they vanish for μ approaching the linear limit, ε. We numerically solved Eqs. (11), using the Newton's method in the frequency domain. In Fig. 3(c), the consideration of the vicinity of the zero point suggests that, for the same displacement of k_z away from the Weyl points, the right- and left-side modes possess the same characteristics except for the fact that soliton solutions emerge at opposite signs of the nonlinearity. The nonlinear surface states are characterized by dependence of the total norm $U=U_A+U_B$ of the A and B wave component per z-period on μ, where $U_\sigma=\int_{-L/2}^{L/2}dz\iint\left|\psi_\sigma(x,y)\right|^2dxdy$ are norms of the two components per z-period. The evidence that nonlinear states bifurcate from the linear ones is provided by dependencies of the peak amplitudes, $\max\left|\psi_\sigma\right|$, on μ. The vanishing of $\max\left|\psi_\sigma\right|$ at the bifurcation point indicates the thresholdless character of the nonlinear surface states. In addition, amplitude profiles of nonlinear modes $\psi_\sigma^{\mathrm{RT(LT)}}$ for different types of the nonlinearity, localized at the A-B site sets are shown in Fig. 3(d). It is seen that the modes are almost identical, except for being localized at different corner of the lattice. Therefore, it is sufficient to analyze the single species of the modes. Thus we suppress the superscript RT(LT), and focus on the mode attached to right corner. The existence interval of μ for nonlinear modes is determined by energy difference $\delta=\varepsilon-\mu$ between the linear and nonlinear state for given k_z. This difference, representing the energy separation from the bulk modes, means, as mentioned above, that the nonlinear states, localized along the z-axis, may only exist with μ falling into a gap of the spectral structure. When μ crosses the edge of the spectral band, the nonlinear mode will lose the localization and couple with the bulk modes (embedded solitons, which may exist, as exceptional states, in Bloch bands of some discrete nonlinear systems [65], were not found here).

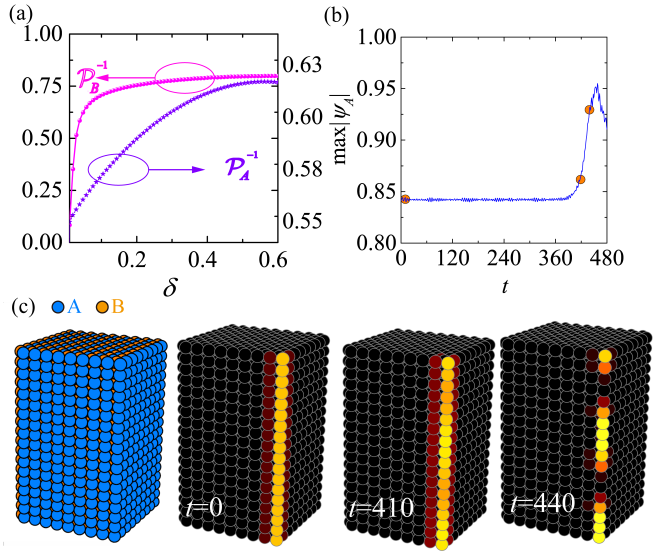

FIG. 4. (a) The inverse participation number $\mathcal{P}_\sigma{}^{-1}$ versus energy difference δ corresponding to different sites. (b) The stable evolution of perturbed nonlinear surface states corresponding to $\mu=0.1$ and $k_z=0.6\pi$. The evolution of peak amplitudes $\max|\psi_A|$ in t testifies to the stability of the nonlinear wavepacket. (c) The distribution of the A and B sites and the evolution pattern of ψ_σ versus t, displayed in the 3D form.

To quantify the soliton's localization, we use the inverse participation number:

$$\mathcal{P}_\sigma{}^{-1}=\int_{-L/2}^{L/2}dz\iint|\psi_\sigma|^4dxdy\Big/\left(\int_{-L/2}^{L/2}dz\iint|\psi_\sigma|^2dxdy\right)^2. \quad (12)$$

Figure 4(a) plots δ versus the inverse participation number $\mathcal{P}_\sigma{}^{-1}$, the colored lines pertaining to different sites A and B. With the increasing of δ, the localization monotonically strengthens with the increase of $\mathcal{P}_\sigma{}^{-1}$.

Figure 4(b) reports results of the stability analysis for the nonlinear surface states, performed by perturbing them with a small broadband input noise (1% in amplitude), and continuously tracing their subsequent evolution up to very large times. It is seen that the perturbed nonlinear modes maintain themselves even at $t > 360$. Eventually, the nonlinear surface states are unstable due to the modulation instability in the periodic potential [21, 66]. However, rather than decaying, the z-periodic periodic surface state breaks up into soliton trains (see the pattern at $t = 440$ in Fig. 4(c)). These results suggest that the nonlinearity may indeed build robust surface Weyl solitons, bifurcating from linear surface states in the Weyl lattice. To develop a more regular approach for demonstrating the existence of the Weyl solitons, we rewrite Eqs. 8 as $i\partial\mathbf{\Psi}/\partial t = \mathcal{L}\mathbf{\Psi}+\mathcal{N}\mathbf{\Psi}$, where $\mathbf{\Psi} = (\psi_A, \psi_B)^T$, operator $\mathcal{L} = H$ includes all linear terms, while operator $\mathcal{N}$ accounts for the nonlinearity. Then, the expression of the soliton can be written as [67]

$$\mathbf{\Psi}(x,y,z,t) = \sum_j \int_{-\pi/L}^{\pi/L} a_j(\kappa,t)\,\mathbf{u}(x,y,z,k_z+\kappa)\,e^{i\varepsilon t+i(k_z+\kappa)z}d\kappa \approx \int_{-\pi/L}^{\pi/L} a(\kappa,t)\,\mathbf{u}(x,y,z,k+\kappa)\,e^{i\varepsilon t+i(k_z+\kappa)z}d\kappa, \tag{13}$$

where vector function $\mathbf{u} = (u_A, u_B)^T$ satisfies the linear Eq. $(\mathcal{L}+\varepsilon)\,\mathbf{u}e^{ik_z z} = 0$ for the linear Bloch mode with momentum k_z, and we take into account that the corresponding energy, ε, depends on quasi-momentum k_z. Here κ is the momentum offset from the carrier soliton momentum k_z, and amplitude $a(\kappa,t)$ is assumed to be well localized in κ. Using the Taylor expansion in κ for $\mathbf{u}(x,y,z,k_z+\kappa)$ in the above integral, one obtains the expression for the shape of the surface-state wave packet:

$$\mathbf{\Psi}(x,y,z,t) = e^{i\varepsilon t+ik_z z}\sum_{j=0,\infty}\frac{(-i)^j}{j!}\frac{\partial^j\mathbf{u}}{\partial {k_z}^j}\left[\frac{\partial^j a(z,t)}{\partial z^j}\right], \tag{14}$$

where $a(z,t) = \int_{-\pi/L}^{\pi/L} a(\kappa,t)\,e^{ik_z z}d\kappa$ is the envelope function of the corresponding nonlinear surface state. To see how $\mathcal{L}$ acts on wave function $\mathbf{\Psi}$, we move $\mathcal{L}$ through the integral and take $\mathcal{L}\mathbf{u}e^{ik_z z} = -\varepsilon\mathbf{u}e^{ik_z z}$ into account, arriving at

$$\mathcal{L}\mathbf{\Psi} = -\int_{-\pi/L}^{\pi/L}\varepsilon(k_z+\kappa)\,a(\kappa,t)\,\mathbf{u}(x,y,z,k_z+\kappa)\,e^{i\varepsilon t+i(k_z+\kappa)z}d\kappa. \tag{15}$$

Employing the Taylor series expansion in κ for both $\varepsilon(k_z+\kappa)$ and $\mathbf{u}(x,y,z,k_z+\kappa)$, we further obtains

$$\mathcal{L}\mathbf{\Psi} = -e^{i\varepsilon t+ik_z z}\sum_{j=0,\infty}\frac{(-i)^j}{j!}\frac{\partial^j(\varepsilon\mathbf{u})}{\partial {k_z}^j}\left[\frac{\partial^j a(z,t)}{\partial z^j}\right]. \tag{16}$$

Assuming that $\mathbf{u}$ changes with k_z much slower than eigenvalue ε, the slowly-varying-amplitude approximation results in the envelope of a forward-travelling wave, slowly varying in time and space compared to the underlying period, and the underlying solution can be obtained in the approximate form, eliminating terms with higher-order partial derivatives. This approximation allows us to keep only the $j = 0$ term in Eqs. 14, so that $\mathbf{\Psi}(x,y,z,t) = e^{i\varepsilon t+ik_z z}\mathbf{u}(x,y,z,t)\,a(z,t)$ and $\partial^j(\varepsilon\mathbf{u})/\partial {k_z}^j \approx \mathbf{u}\partial^j\varepsilon/\partial {k_z}^j$, while the nonlinear term $\mathcal{N}$ simplifies to $a|a|^2\mathbf{u}e^{i\varepsilon t+ik_z z}$. Finally, we multiply Eq. $i\partial\mathbf{\Psi}/\partial t = \mathcal{L}\mathbf{\Psi}+\mathcal{N}\mathbf{\Psi}$ by $\mathbf{u}^\dagger$ and integrate it over one period along the z-axis and over the entire (x,y) plane,

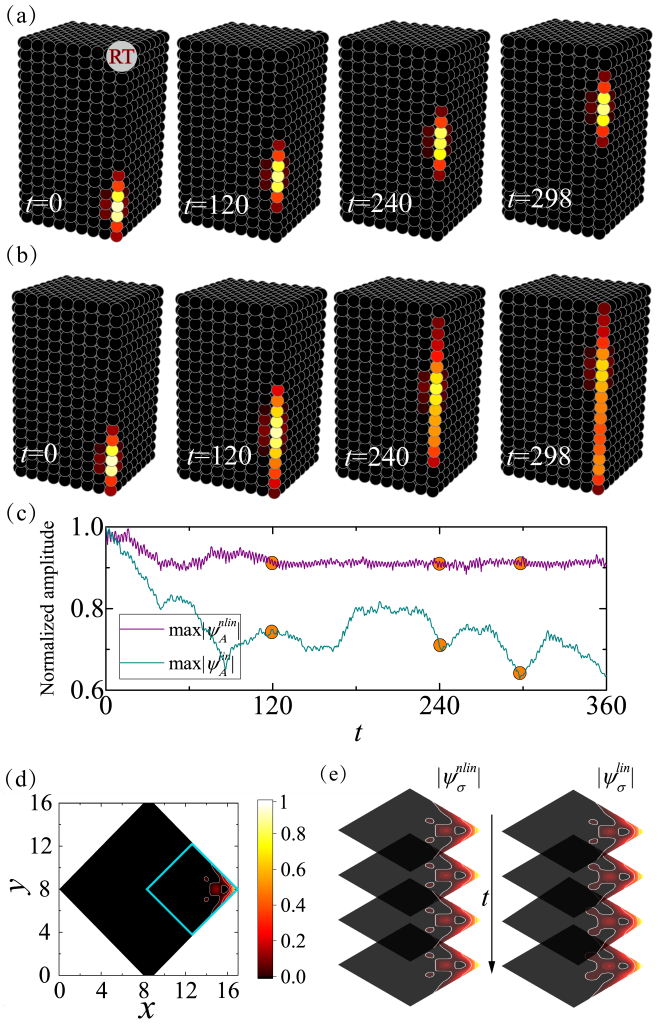

FIG. 5. The propagation of a nonlinear wavepacket at $\delta = 0.12$. To stress the fact that the surface state moves along the z-direction, and to provide details of its shape, we show distributions of ψ_A in the 3D window at times $t = 0; 120; 240; 298$. (a) At the initial moment, $t = 0$, the input beam is localized at the surface with $k_z = 0.6\pi$. The wavepacket moves along the z-axis on the left or right side of the bulk lattice. The shape of the wavepacket is preserved, under the action of the nonlinearity. (b) With the same input, the wavepacket is deformed in the course of the evolution without the nonlinearity. (c) The dependence of the peak amplitude of the ψ_A component on t for the linear and nonlinear systems, with the orange circles representing the time moments used in Figs. 5(a) and (b). (d) The panel shows normalized isocontours of the density of $|\psi_\sigma|$. (e) Zoomed evolution in the cyan square in Fig. 5(d), with or without the nonlinearity.

which allows us to derive the nonlinear Schrödinger Eq. for the envelope function:

$$i\frac{\partial a}{\partial t}=i\varepsilon'\frac{da}{dz}+\frac{1}{2}\varepsilon''\frac{d^2a}{dz^2}+g_{\text{eff}}\left|a\right|^2a. \tag{17}$$

Here, we keep only the first two terms proportional to $\varepsilon'=\partial\varepsilon/\partial k_z$ and $\varepsilon''=\partial^2\varepsilon/\partial {k_z}^2$ in the Taylor expansion of $\varepsilon\left(k_z\right)$. The effective nonlinear coefficient is $g_{\text{eff}}=\iiint\mathbf{u}^\dagger\mathcal{N}\mathbf{u}dxdydz/\iiint\mathbf{u}^\dagger\mathbf{u}dxdydz$. This coefficient can be calculated numerically for different values of k_z, using the linear Bloch modes. When $\varepsilon''>0$ [which corresponds to the red square in Fig. 3(a)], Eq. (17) admits the bright-soliton solution:

$$a_{\text{bright}}\left(z,t\right)=\left(2\delta/g_{\text{eff}}\right)^{1/2}\text{sech}\left[\left(2\delta\Big/\varepsilon''\right)^{1/2}\left(z+\varepsilon't\right)\right]e^{-i\delta t}. \tag{18}$$

Note that the energy shift δ in Eq. (18), introduced by the nonlinearity, leads to the consequence that the total wave function $\mathbf{\Psi}\left(x,y,z\right)=e^{i\varepsilon t+ik_zz}\mathbf{u}\left(x,y,z,k_z\right)a\left(z,t\right)$ varies as $e^{-i\mu t}$. The shift serves as a compensation parameter for the energy difference between the bulk and nonlinear modes, which are used as the complete set of nonlinear wave functions. Figure 5(a) shows the evolution of solitons constructed as per Eqs. (14) with the envelope function given by Eq. (18). At the chosen value of k_z, dispersion ε'' and eigenstate $\mathbf{u}$ were found by numerically solving the eigenvalue problem defined by Eqs. (7). In this context, periodic boundary conditions along z axis were used.

A Weyl soliton, that starts its evolution being localized at the right side of the Weyl lattice features unidirectional motion. This can be interpreted as follows: unidirectional transport of surface modes relies on the global topology of the lattice, as a consequence of its specific topological protected band structure, while the localization of the wave packet is governed by the nonlinearity. One can see that, after an initial transient period, when the peak amplitude of the input wave form decreases due to internal reshaping of its profile, the soliton's amplitude of soliton remains almost constant [see the purple curve in Fig. 5(d) showing the evolution of the peak amplitude $\max\left|\psi_A\right|$ of the ψ_A component], with the velocity which is nearly identical to ε'. Sets of similar long-lived nonlinear surface states can be generated, varying the respective value of k_z. To confirm that the localized states indeed exist due to the nonlinearity, we used the same input, while nonlinearity was switched off. Figure 5(b) shows snapshots of the dynamics associated with the surface states in the absence of the nonlinearity. We observe expansion of the wave packet in Fig. 5(b) and decay of its amplitude, as shown by the green curve in Fig. 5(c). In addition, we introduce the 2D cross section of the 3D domain at the central position of the wave packet in the z direction, and display the density of $\left|\psi_\sigma\right|$ by means of isocontours in the 2D plane, in Fig. 5(c), for the same four time moments that were chosen in Fig. 5(e). It is observed that snapshots of the nonlinear mode maintained their shape, while the linear mode is spreading out.

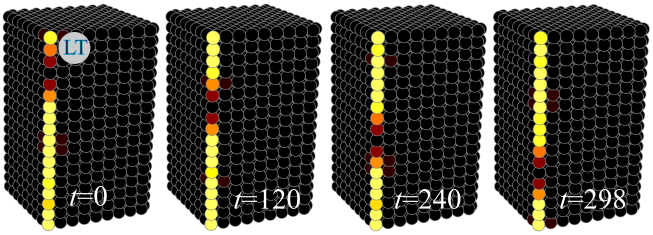

FIG. 6. The stable evolution of the dark soliton in the nonlinear system is shown for $\delta=-0.12$ and $k_z=-0.4\pi$. The dark spot moves without any notable deformation.

In addition, for $\varepsilon''<0$ [which corresponds to the blue circle in Fig. 3(a)], the system gives rise to dark solitons, with the envelope:

$$a_{\text{dark}}\left(z,t\right)=\left(-2\delta/g_{\text{eff}}\right)^{1/2}\tanh\left[\left(-2\delta\Big/\varepsilon''\right)^{1/2}\left(z+\varepsilon't\right)\right]e^{i\delta t}. \tag{19}$$

In Fig. 6, we show the evolution of the surface state constructed using this envelope and Bloch modes $\mathbf{u}$. In the simulations, the dark soliton also survives for a long time, keeping its initial shape and propagating along an opposite direction of the bight one.

IV. CONCLUSION

The aim of this work is to demonstrate the existence of topological Weyl surface solitons in the 3D optical lattice. To the best of our knowledge, effects of the nonlinear were not previously studied in settings emulating Weyl semimetals by dint of the appropriately designed optical lattice with an ultracold atomic gas loaded into it. This proposal also offers a new feasible control of the particles governed by Weyl Eq., which may conquer the difficulty of physical realization in the real material. Robust modes in the form of Weyl solitons are revealed by the systematic analysis of the 3D nonlinear model. Note that the Weyl solitons arising here should be distinguished from gap solitons. Being formed from topological surface modes, the Weyl solitons can only propagate along surfaces of the lattice, in contrast to gap solitons, which propagate in the bulk. The Weyl-soliton states bifurcate from linear surface modes at zero intensity, indicating the absence of any threshold necessary for their existence. In addition, bright and dark Weyl soliton perform an intriguing counter-propagation unidirectional characteristics. Furthermore, the analysis developed in this work is also applicable to optical waveguides [68, 69] and nanowires [70, 71] which may support Weyl solitons, therefore making our results very general and of relevance to the systems beyond optical lattices. In closing, Weyl solitons, the last member of the topological soliton family, may pave the way for the realization of many fascinating topological nonlinear phenomena.

FUNDING INFORMATION

National Natural Science Foundation of China (NSFC) (61475101); Innovation Program of Shanghai Municipal Education Commission (13ZZ022); the joint program in physics between NSF and Binational (US-Israel) Science Foundation (project No. 2015616); Israel Science Foundation (grant No. 1286/17).

ACKNOWLEDGMENTS

Special thanks to Xianfeng Chen and Fangwei Ye for discussion.

[1] K. Nomura and A. H. MacDonald, "Quantum transport of massless Dirac fermions," Physical Review Letters **98**, 076602 (2007).

[2] L. Fu and C. L. Kane, "Probing neutral Majorana fermion edge modes with charge transport," Physical Review Letters **102**, 216403 (2009).

[3] J. P. Xu, M. X. Wang, Z. L. Liu, J. F. Ge, X. Yang, C. Liu, Z. A. Xu, D. Guan, C. L. Gao, D. Qian, Y. Liu, Q. H. Wang, F. C. Zhang, Q. K. Xue, and J. F. Jia, "Experimental detection of a Majorana mode in the core of a magnetic vortex inside a topological insulator-superconductor Bi_2Te_3/ $NbSe_2$ heterostructure," Physical Review Letters **114**, 017001 (2015).

[4] S. M. Huang, S. Y. Xu, I. Belopolski, C. C. Lee, G. Chang, B. Wang, N. Alidoust, G. Bian, M. Neupane, C. Zhang, S. Jia, A. Bansil, H. Lin, and M. Z. Hasan, "A Weyl Fermion semimetal with surface Fermi arcs in the transition metal monopnictide TaAs class," Nature Communications **6**, 7373 (2015).

[5] Lv, B. Q. and Weng, H. M. and Fu, B. B. and Wang, X. P. and Miao, H. and Ma, J. and Richard, P. and Huang, X. C. and Zhao, L. X. and Chen, G. F. and Fang, Z. and Dai, X. and Qian, T. and Ding, H., "Experimental discovery of Weyl semimetal TaAs," Physical Review X **5**, 031013 (2015).

[6] S.-Y. Xu, I. Belopolski, N. Alidoust, M. Neupane, G. Bian, C. Zhang, R. Sankar, G. Chang, Z. Yuan, C.-C. Lee, S.-M. Huang, H. Zheng, J. Ma, D. S. Sanchez, B. Wang, A. Bansil, F. Chou, P. P. Shibayev, H. Lin, S. Jia, and M. Z. Hasan, "Discovery of a Weyl fermion semimetal and topological Fermi arcs," Science **349**, 613–617 (2015).

[7] W. J. Chen, M. Xiao, and C. T. Chan, "Photonic crystals possessing multiple Weyl points and the experimental observation of robust surface states," Nature Communications **7**, 13038 (2016).

[8] Q. Lin, M. Xiao, L. Yuan, and S. Fan, "Photonic Weyl point in a two-dimensional resonator lattice with a synthetic frequency dimension," Nature Communications **7**, 13731 (2016).

[9] L. Lu, L. Fu, J. D. Joannopoulos, and M. Soljai, "Weyl points and line nodes in gyroid photonic crystals," Nature Photonics **7**, 294–299 (2013).

[10] L. Lu, Z. Wang, D. Ye, L. Ran, L. Fu, J. D. Joannopoulos, and M. Soljai, "Experimental observation of Weyl points," Science **349**, 622–624 (2015).

[11] W. Gao, B. Yang, M. Lawrence, F. Fang, B. Béri, and S. Zhang, "Photonic weyl degeneracies in magnetized plasma," Nature communications **7** (2016).

[12] N. Goldman, J. Dalibard, A. Dauphin, F. Gerbier, M. Lewenstein, P. Zoller, and I. B. Spielman, "Direct imaging of topological edge states in cold-atom systems," Proceedings of the National Academy of Sciences **110**, 6736–6741 (2013).

[13] A. Celi, P. Massignan, J. Ruseckas, N. Goldman, I. B. Spielman, G. Juzeliūnas, and M. Lewenstein, "Synthetic gauge fields in synthetic dimensions," Physical Review Letters **112**, 043001 (2014).

[14] A. Nalitov, D. Solnyshkov, and G. Malpuech, "Polariton Z topological insulator," Physical Review Letters **114**, 116401 (2015).

[15] S. Ganeshan and S. D. Sarma, "Constructing a Weyl semimetal by stacking one-dimensional topological phases," Physical Review B **91**, 125438 (2015).

[16] Z. Lan, N. Goldman, A. Bermudez, W. Lu, and P. hberg, "Dirac-Weyl fermions with arbitrary spin in two-dimensional optical superlattices," Physical Review B **84**, 165115 (2011).

[17] A. Weststrom and T. Ojanen, "Designer curved-space geometry for relativistic fermions in weyl metamaterials," Physical Review X **7**, 041026 (2017).

[18] M. Saffman, T. G. Walker, and K. Mlmer, "Quantum information with Rydberg atoms," Reviews of Modern Physics **82**, 2313 (2010).

[19] H. Gibbs, *Optical bistability: controlling light with light* (Elsevier, 2012).

[20] Y. V. Kartashov, B. A. Malomed, and L. Torner, "Solitons in nonlinear lattices," Reviews of Modern Physics **83**, 247 (2011).

[21] F. Lederer, G. I. Stegeman, D. N. Christodoulides, G. Assanto, M. Segev, and Y. Silberberg, "Discrete solitons in optics," Physics Reports **463**, 1–126 (2008).

[22] T. Dauxois and M. Peyrard, *Physics of solitons* (Cambridge University, 2006).

[23] J. Yang, *Nonlinear waves in integrable and nonintegrable systems* (SIAM, 2010).

[24] Y.-R. Shen, "The principles of nonlinear optics," New York, Wiley-Interscience **1**, 575 (1984).

[25] E. J. Meier, F. A. An, and B. Gadway, "Observation of the topological soliton state in the Su-Schrieffer-Heeger model," Nature Communications **7**, 13986 (2016).

[26] D. Leykam and Y. D. Chong, "Edge solitons in nonlinear-photonic topological insulators," Physical Review Letters **117**, 143901 (2016).

[27] Y. V. Kartashov and D. V. Skryabin, "Modulational instability and solitary waves in polariton topological insulators," Optica **3**, 1228–1236 (2016).

[28] M. Quiroga-Teixeiro and H. Michinel, "Stable azimuthal stationary state in quintic nonlinear optical media,"

JOSA B **14**, 2004–2009 (1997).

[29] P. Kevrekidis, H. Susanto, R. Carretero-González, B. Malomed, and D. Frantzeskakis, "Vector solitons with an embedded domain wall," Physical Review E **72**, 066604 (2005).

[30] R. Carretero-González, D. Frantzeskakis, and P. Kevrekidis, "Nonlinear waves in Bose–Einstein condensates: physical relevance and mathematical techniques," Nonlinearity **21**, R139 (2008).

[31] F. K. Abdullaev, A. Gammal, M. Salerno, and L. Tomio, "Localized modes of binary mixtures of Bose-Einstein condensates in nonlinear optical lattices," Physical Review A **77**, 023615 (2008).

[32] A. S. Reyna, K. C. Jorge, and C. B. de Araújo, "Two-dimensional solitons in a quintic-septimal medium," Physical Review A **90**, 063835 (2014).

[33] G. Spagnolli, G. Semeghini, L. Masi, G. Ferioli, A. Trenkwalder, S. Coop, M. Landini, L. Pezzè, G. Modugno, M. Inguscio, A. Smerzi, and M. Fattori, "Crossing over from attractive to repulsive interactions in a tunneling bosonic josephson junction," Physical Review Letters **118**, 230403 (2017).

[34] Y.-J. Lin, R. L. Compton, K. Jimenez-Garcia, J. V. Porto, and I. B. Spielman, "Synthetic magnetic fields for ultracold neutral atoms," Nature **462**, 628–632 (2009).

[35] J. Dalibard, F. Gerbier, G. Juzeliūnas, and P. Öhberg, "Colloquium: Artificial gauge potentials for neutral atoms," Reviews of Modern Physics **83**, 1523 (2011).

[36] J. Cuevas-Maraver, P. G. Kevrekidis, A. Saxena, A. Comech, and R. Lan, "Stability of solitary waves and vortices in a 2D nonlinear Dirac Model," Physical Review Letters **116**, 214101 (2016).

[37] P. Zou, J. Brand, X.-J. Liu, and H. Hu, "Traveling majorana solitons in a low-dimensional spin-orbit-coupled fermi superfluid," Physical Review Letters **117**, 225302 (2016).

[38] M. S. Rudner and L. S. Levitov, "Topological transition in a non-Hermitian quantum walk," Physical Review Letters **102**, 065703 (2009).

[39] D. R. Hofstadter, "Energy levels and wave functions of Bloch electrons in rational and irrational magnetic fields," Physical Review B **14**, 2239 (1976).

[40] T. Dubcek, C. J. Kennedy, L. Lu, W. Ketterle, M. Soljacic, and H. Buljan, "Weyl points in three-dimensional optical lattices: Synthetic magnetic monopoles in momentum space," Physical Review Letters **114**, 225301 (2015).

[41] A. Eckardt, "Colloquium: Atomic quantum gases in periodically driven optical lattices," Reviews of Modern Physics **89**, 011004 (2017).

[42] D. Jaksch and P. Zoller, "Creation of effective magnetic fields in optical lattices: the hofstadter butterfly for cold neutral atoms," New Journal of Physics **5**, 56 (2003).

[43] H. Miyake, G. A. Siviloglou, C. J. Kennedy, W. C. Burton, and W. Ketterle, "Realizing the harper hamiltonian with laser-assisted tunneling in optical lattices," Physical Review Letters **111**, 185302 (2013).

[44] R. Qi and H. Zhai, "Bound states and scattering resonances induced by spatially modulated interactions," Physical Review Letters **106**, 163201 (2011).

[45] Cappellini, G. and Mancini, M. and Pagano, G. and Lombardi, P. and Livi, L. and Siciliani de Cumis, M. and Cancio, P. and Pizzocaro, M. and Calonico, D. and Levi, F. and Sias, C. and Catani, J. and Inguscio, M. and Fallani, L., "Direct observation of coherent interorbital spin-exchange dynamics," Physical Review Letters **113**, 120402 (2014).

[46] Bleu, O and Malpuech, G and Solnyshkov, DD, "$\mathbb{Z}_2$ topological insulator analog for vortices in an interacting bosonic quantum fluid," arXiv:1709.01830 (2017).

[47] Y. He, J. Moore, and C. Varma, "Berry phase and anomalous hall effect in a three-orbital tight-binding hamiltonian," Physical Review B **85**, 155106 (2012).

[48] K. W. Kim, W.-R. Lee, Y. B. Kim, and K. Park, "Surface to bulk Fermi arcs via Weyl nodes as topological defects," Nature Communications **7**, 13489 (2016).

[49] R. Golizadeh-Mojarad and S. Datta, "Nonequilibrium Greens function based models for dephasing in quantum transport," Physical Review B **75**, 081301 (2007).

[50] L. Huang, Z. Meng, P. Wang, P. Peng, S.-L. Zhang, L. Chen, D. Li, Q. Zhou, and J. Zhang, "Experimental realization of two-dimensional synthetic spin-orbit coupling in ultracold fermi gases," Nature Physics **12**, 540–544 (2016).

[51] Z. Meng, L. Huang, P. Peng, D. Li, L. Chen, Y. Xu, C. Zhang, P. Wang, and J. Zhang, "Experimental observation of a topological band gap opening in ultracold fermi gases with two-dimensional spin-orbit coupling," Physical Review Letters **117**, 235304 (2016).

[52] A. Burkov and L. Balents, "Weyl semimetal in a topological insulator multilayer," Physical Review Letters **107**, 127205 (2011).

[53] M. Xiao, W.-J. Chen, W.-Y. He, and C. T. Chan, "Synthetic gauge flux and weyl points in acoustic systems," Nature Physics **11**, 920–924 (2015).

[54] Y. Kim, B. J. Wieder, C. Kane, and A. M. Rappe, "Dirac line nodes in inversion-symmetric crystals," Physical Review Letters **115**, 036806 (2015).

[55] K. Mullen, B. Uchoa, and D. T. Glatzhofer, "Line of dirac nodes in hyperhoneycomb lattices," Physical Review Letters **115**, 026403 (2015).

[56] L.-K. Lim and R. Moessner, "Pseudospin vortex ring with a nodal line in three dimensions," Physical Review Letters **118**, 016401 (2017).

[57] S. Kumar, A. M. Perego, and K. Staliunas, "Linear and nonlinear bullets of the Bogoliubov-de Gennes excitations," Physical Review Letters **118**, 044103 (2017).

[58] T. R. Melvin, A. R. Champneys, P. G. Kevrekidis, and J. Cuevas, "Radiationless traveling waves in saturable nonlinear Schrodinger lattices," Physical Review Letters **97**, 124101 (2006).

[59] K. Li, L. Deng, E. W. Hagley, M. G. Payne, and M. Zhan, "Matter-wave self-imaging by atomic center-of-mass motion induced interference," Physical Review Letters **101**, 250401 (2008).

[60] J. Zhu, G. Dong, M. N. Shneider, and W. Zhang, "Strong local-field effect on the dynamics of a dilute atomic gas irradiated by two counterpropagating optical fields: Beyond standard optical lattices," Physical Review Letters **106**, 210403 (2011).

[61] G. Dong, J. Zhu, W. Zhang, and B. A. Malomed, "Polaritonic solitons in a bose-einstein condensate trapped in a soft optical lattice," Physical Review Letters **110**, 250401 (2013).

[62] D. Christodoulides and R. Joseph, "Discrete self-focusing in nonlinear arrays of coupled waveguides," Optics Letters **13**, 794–796 (1988).

[63] J. Hudock, N. K. Efremidis, and D. N. Christodoulides, "Anisotropic diffraction and elliptic discrete solitons in two-dimensional waveguide arrays," Optics Letters **29**, 268–270 (2004).

[64] T. I. Vanhala, T. Siro, L. Liang, M. Troyer, A. Harju, and P. Trm, "Topological phase transitions in the repulsively interacting Haldane-Hubbard model," Physical Review Letters **116**, 225305 (2016).

[65] K. Yagasaki, A. R. Champneys, and B. A. Malomed, "Discrete embedded solitons," Nonlinearity **18**, 2591 (2005).

[66] J. Meier, G. Stegeman, D. Christodoulides, Y. Silberberg, R. Morandotti, H. Yang, G. Salamo, M. Sorel, and J. Aitchison, "Experimental observation of discrete modulational instability," Physical Review Letters **92**, 163902 (2004).

[67] M. J. Ablowitz, *Nonlinear dispersive waves: asymptotic analysis and solitons*, vol. 47 (Cambridge University, 2011).

[68] F. Dreisow, M. Heinrich, R. Keil, A. Tünnermann, S. Nolte, S. Longhi, and A. Szameit, "Classical simulation of relativistic Zitterbewegung in photonic lattices," Physical Review Letters **105**, 143902 (2010).

[69] R. Keil, C. Noh, A. Rai, S. Stützer, S. Nolte, D. G. Angelakis, and A. Szameit, "Optical simulation of charge conservation violation and Majorana dynamics," Optica **2**, 454–459 (2015).

[70] Y. Oreg, G. Refael, and F. von Oppen, "Helical liquids and majorana bound states in quantum wires," Physical Review Letters **105**, 177002 (2010).

[71] A. Das, Y. Ronen, Y. Most, Y. Oreg, M. Heiblum, and H. Shtrikman, "Zero-bias peaks and splitting in an alinas nanowire topological superconductor as a signature of majorana fermions," Nature Physics **8**, 887 (2012).